sialidase [14, 15]. *N*-Stearoyl glycolipids, as standards for TLC-densitometry, were prepared by deacylation with sphingolipid ceramide N-deacylase (Pseudomonas sp., Tk4), followed by reacylation with stearoyl chloride. Polyclonal antibodies to LJ, GA1, GM1 and Forssman glycolipids, and monoclonal antibodies to FGA1 (LFA-1), FGM1 (LFM-1), and sulfatides (TCS-1) were generated in our laboratory by immunizing rabbits or mice with LJ or purified glycolipids together with *Mycobacterium tuberculosis* or *Salmonella minnesota* as the adjuvant [5].

Analysis of lipids

Total lipids were extracted from the lyophilized tissues and contents with chloroform/methanol/water (20:10:1, 10:20:1 and 1:1:0, by vol.), and the combined extracts were used as the total lipids. A part of each extract was applied to a DEAE-Sephadex column (A-25, acetate form; GE Healthcare Bioscience, Piscataway, NJ, USA), and the unabsorbed and absorbed fractions were desalted by dialysis, being used as neutral and acidic lipids, respectively. Also, the neutral glycolipids were separated from the neutral lipids by acetylation, separation of the acetylated derivatives, deacetylation and desalting, whereas the acidic glycolipids were prepared from the acidic lipids by saponification with 0.5 M NaOH in methanol [16].

The total, acidic and neutral lipids, and acidic and neutral glycolipids thus obtained were applied on plastic-coated (Macherey-Nagel, Düren, Germany) and glass-coated (Merck, Darmstadt, Germany) TLC plates, which were then developed with n-hexane/diethylether/acetic acid (80:30:4, by vol.) for neutral lipids, chloroform/methanol/water (65:25:4, by vol.) for bacterial glycolipids and (65:35:8, by vol.) for neutral glycosphingolipids, chloroform/methanol/0.5% $CaCl_2$ in water (55:45:10, by vol.) for acidic glycolipids, and chloroform/methanol/acetone/acetic acid/water (8:2:4:2:1, by vol.) for cholesterol sulfate (CS) and sulfated glycolipids, and the spots were visualized with cupric acetate-phosphoric acid for neutral lipids, phospholipids and CS, Dittmer's reagent for phospholipids, and orcinol-sulfuric acid reagent for glycolipids. The densities of spots on TLC plates were determined by image analysis (NIH image). Standard lipids (0.1 to 1.5 μg), *i.e. N*-stearoyl derivatives of GlcCer, LacCer, Gb_3Cer, Gb_4Cer, Forssman glycolipid and GA1, FGM1, FGA1, triolein, oleic acid, cholesterol, sodium taurocholate and CS, were developed on the same TLC plates for the preparation of standard curves [5, 16].

Structural analysis of glycolipids

The individual glycolipids were purified using a silica gel (Iatrobeads 6RS8060; Iatron Laboratory, Tokyo) column by gradient elution with chloroform/isopropyl alcohol/water (85:15:0.2 and 40:60:2, by vol.) The purified ceramide monohexosides (CMH), diacylglyceryl dihexosides (DHDG), GA1 and sulfated GA1 (SGA1, IV^3SO_3-Gg_4Cer) were analyzed by negative ion FABMS (JMS-700 TKM; JEOL, Tokyo) with triethanolamine as the matrix solvent. For determination of the compositions of fatty acids and carbohydrates, they were methanolized with 5% HCl in methanol at 80°C for 16 h. The resulting fatty acid methyl esters were extracted with n-hexane, and 1-*O*-methyl hexoses in the methanol phase were converted to trimethylsilyl derivatives with pyridine/hexamethyl disilazane/trimethylchlorosilane (10:2:1, by vol.) at 60°C for 5 min, followed by analysis with a GLC-mass spectrometer equipped with a DB-1 column (0.25 mmø×30 m) (Shimadzu, Kyoto). For characterization of SGA1, it was solvolyzed with 9 mM sulfuric acid in dimethyl sulfoxide/methanol (9:1, by vol.) at 80°C for 1 h, and the product was detected by TLC-immunostaining with anti-GA1 antiserum. Also, linkage analysis of carbohydrates was carried out by conversion of glycolipids to partially methylated aldohexitol acetates and *N*-methyl acetoamido aldohexitol acetates, followed by analysis with a GLC-mass spectrometer [16].

TLC-immunostaining

Lipids were developed on plastic-coated TLC plates (Macherey-Nagel), which were then blocked with blocking buffer (PBS containing 1% polyvinylpyrrolidone and 1% ovalbumin), and the spots were visualized by immunostaining with the above anti-LJ antibodies (1:500) diluted with dilution buffer (PBS containing 3% polyvinylpyrrolidone), followed by immunostaining with peroxidase-conjugated anti-rabbit IgG and IgM (1:1000; Jackson Immunoresearch Lab., PA, USA), and peroxidase substrates, 4-chloro-1-naphthol and H_2O_2, according to the procedure reported previously [5, 16].

Sequence of bacterial 16S-rRNA

Bacteria picked up with a toothpick were treated with proteinase K (10 mg/μl), EDTA (5 mM), NaCl (400 mM), and SDS (0.3%) in 20 mM Tris-HCl buffer (pH 8.0) at 55°C for 2 h, and the resultant DNAs were used for PCR with DNA polymerase (NovaTaq™ Hot Start DNA polymerase; Novagen, San Diego, CA, USA) in Ampdirect Plus (Shimadzu, Kyoto) under the following conditions: 27f sense primer, AGAGTTTGATCCTGGCTCAG, 1544r antisense primer, AGAAAGGAGGTGATCCAGCC, 95°C, 10 min, followed by 35 cycles of 94°C for 30 s, 53°C for 1 min and 72°C for 1 min, and then 72°C for 7 min [17]. The PCR products were purified with a MinElute PCR Purification Kit (Qiagen, MD, USA), and their sequences

were determined with a DNA analysis system with BigDye® Terminator Cycle Sequencing Reagent (v. 3.1) according to the manufacturer's instructions (ABI Prism 310 Genetic Analyzer; Applied Biosystems, Foster City, CA, USA).

Results

Region-specific distribution of glycolipids in the murine digestive tract

In accord with our previous report [5], the distribution of glycolipids in the murine digestive tract was found to be region-specific, *i.e.* GA1 in the duodenum, jejunum and ileum, FGM1 in the stomach, and sulfatides in the stomach and cecum (Fig. 1). In addition to these major glycolipids, SGA1 was detected in the duodenum, jejunum and ileum (Fig. 1b and c). The structure of SGA1 was elucidated from the following evidence: positive reaction with anti-sulfatide antibodies (Fig. 1c), positive reaction with anti-GA1 antibodies of the products after solvolysis (Fig. 2), presence of 3-*O*-linked galactose detected on permethylation analysis, and the deprotonated molecular ions of SGA1, and the fragment ions of $[Gg_3Cer\text{-}1]^-$, $[LacCer\text{-}1]^-$, $[GlcCer\text{-}1]^-$, and $[ceramide\text{-}1]^-$ [18]. The extents of sulfation and fucosylation of GA1 were 7.6% and 8.1% in the duodenum, 6.0% and 0.3% in the jejunum, and 4.3% and 9.9% in the ileum, respectively, indicating that more than 85% of GA1 is expressed in these regions. Whereas, in the stomach, cecum and colon, FGA1, but not GA1 or SGA1, was detected, indicating complete fucosylation of GA1 in these regions (Fig. 3). The total amounts and concentrations of epithelial glycolipids and CS in several regions of the murine digestive tract are presented in Table 1. GA1 in the entire small intestine amounted to 674 μg, which was the highest among the glycolipids in these regions. In contrast to the region-specific distributions of GA1, FGA1, SGA1, FGM1 and sulfatide, CMH, Gb_4Cer, Forssman antigen, CS and GM3 were ubiquitously distributed in the digestive tract (Figs. 1 and 3). The tissues containing lipids in the highest amounts were as follows, , jejunum and ileum (CMH, GA1, SGA1 and CS), cecum (FGA1 and sulfatide), and stomach (FGM1) (Table 1).

Glycolipids in the contents of several regions of the murine digestive tract

The gastric contents of eight mice were less than 40% of that of a full stomach, passed through in about 5 h after ingestion, and their dry weights accounted for 6% of the total dried material in the entire digestive tract. The majority of the dried material in the tract were in the cecal and colonic contents, amounting to 35% and 46% of the total, respectively (Table 2). As shown in Fig. 4, triglycerides (TG), free fatty acids (FFA), phosphatidyl ethanolamine (PE), and phosphatidyl choline (PC), all of which were present in the murine food, greatly decreased from the gastric to the ileal contents, and they were almost completely absent in the cecal and colonic contents. In contrast, CMH, which was detected in the murine food and tissues was present in the contents of all regions of the digestive tract, and its relative concentrations in the cecal and colonic contents were higher than those in the gastric, jejunal and ileal contents (Fig. 4d and Table 2). On comparison of the molecular species of CMH in the cecal contents with those in the gastric and jejunal tissues by negative ion FABMS, CMH in the contents was found to be derived from both the gastro-intestinal epithelium and murine food. As shown in Fig. 5, the ceramide moiety of

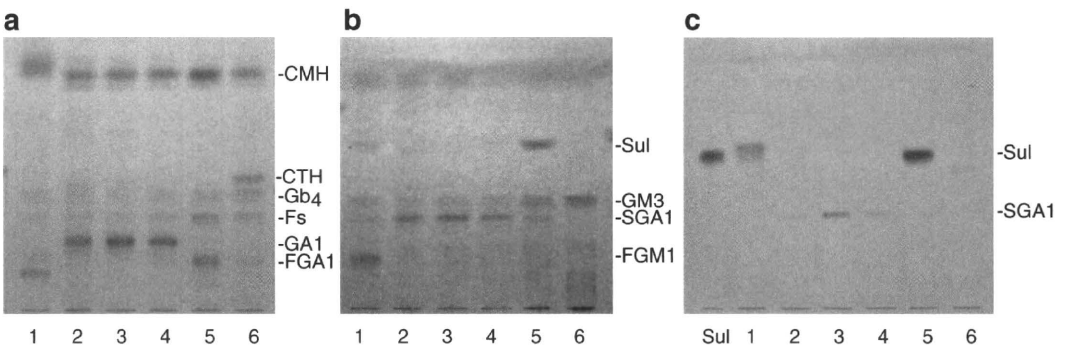

Fig. 1 TLC and TLC-immunostaining of glycolipids from tissues of the murine digestive tract. Neutral (**a**) and acidic (**b** and **c**) glycolipids, corresponding to 0.5 mg dry weight, were developed on plates with chloroform/methanol /water (65:35:8, by vol.) for A, and chloroform/methanol/0.5% $CaCl_2$ in water (55:45:10, by vol.) for B and C, and were detected with orcinol-sulfuric acid reagent for A and B, and with monoclonal anti-sulfatide antibody TCS-1 for C. 1, stomach; 2, duodenum; 3, jejunum; 4, ileum; 5, cecum; 6, colon; Sul, sulfatides; SGA1, $IV^3SO_3\text{-}Gg_4Cer$; CTH, ceramide trihexoside

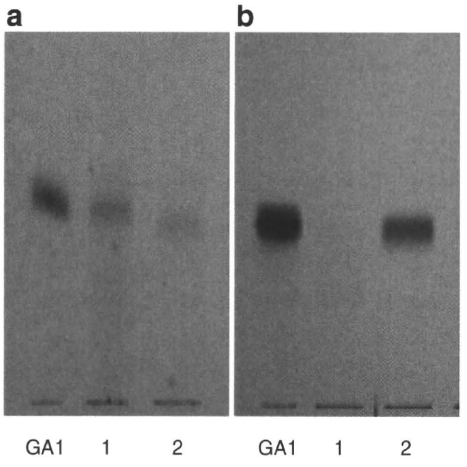

Fig. 2 TLC and TLC-immunostaining of SGA1 from the jejunum. SGA1 isolated from the jejunum (1) and its solvolyzed products (2) were developed with chloroform/methanol/0.5% $CaCl_2$ in water (55:45:10, by vol.), and were detected with orcinol-sulfuric acid reagent (**a**) and by TLC-immunostaining with anti-GA1 antiserum (**b**)

jejunal CMH preferentially comprised of α-hydroxy fatty acyl phytosphingosine: m/z 844, 18t:0–24h:0; m/z 830, 18t:0–23h:0; m/z 816, 18t:0–22h:0; m/z 788, 18t:0–20h:0; and m/z 732, 18t:–16h:0 (Fig. 5b). That of gastric CMH composed of α-hydroxy fatty acyl sphingosine and α-hydroxy fatty acyl phytosphingosine: m/z 872, 18t:0–26h:0; m/z 858, 18t:0–25h:0; m/z 844, 18t:0–24h:0; m/z 826, 18d:1–24h:0; m/z 812, 18d:1–23h:0; m/z 798, 18d:1–22h:0; m/z 770, 18d:1–20h:0; and m/z 714, 18d–16h:0 (Fig. 5a). And that of CMH in the cecal contents composed of a mixture of the above molecular species of gastro-intestinal CMH and CMH in the murine food, which were constituted of nonhydroxy fatty acyl phytosphingosine; m/z 828, 18t:0–24:0; m/z 800, 18t:0–22:0; and m/z 772, 18t:0–18:0 (Fig. 5c). Glucose was a major carbohydrate of CMH in the murine food, as well as that in the tissues and contents, and about 70% and 30% of CMH in the cecal contents was derived from the gastro-intestinal epithelium and murine food, respectively, as estimated from the relative intensities of molecular ions in Fig. 5c. These findings indicate that CMH is stable during the process of digestion and is excreted from the body. Similarly, the other epithelial glycolipids present in the contents were as follows, GA1 and FGA1 in the contents of all regions of the digestive tract, and sulfatides, FGM1 and SGA1 in the contents of the stomach, jejunum and ileum, but not those of the cecum and colon, indicating that the sulfuric and sialic acid groups of sulfatides, FGM1 and SGA1 are removed in the stomach, jejunum and ileum to yield CMH, FGA1 and GA1 in the cecal and colonic contents (Figs. 4d, e, and 6). In the jejunal and ileal contents, GA1 was the major glycolipid, comprising about 60% of the total glycolipids, whose concentration was similar with those in the jejunal and ileal tissues. Also, GA1 and FGA1 in the cecal and colonic contents were present in concentrations of 0.57 μg and 0.02 μg per mg dry weights, and total amounts of 86.2 μg and 3.0 μg, respectively (Table 2). For comparison, the total amounts of several lipids in the contents from different regions of the digestive tract are shown in Fig. 7. PC and free fatty acids from both the murine food and epithelial tissues greatly decreased from the gastric to the ileal contents on enzymatic hydrolysis and incorporation of free fatty acids into the tissues, respectively. Bile acids, which were secreted from the gallbladder and played an essential role in the process of lipid digestion, were the major lipids in the jejunal and ileal contents and, to a lesser extent, in the gastric contents, and were absent in the cecal and colonic contents. Consequently, the major lipids accumulated in the cecal and colonic contents to be excreted from the body were cholesterol, CS, GlcCer, GA1 and FGA1. The total amounts of GA1 and FGA1 in the cecal and colonic contents corresponded to 12.8% and 2.5% of those in the epithelial tissues of the entire digestive tract (Table 1 and Fig. 7).

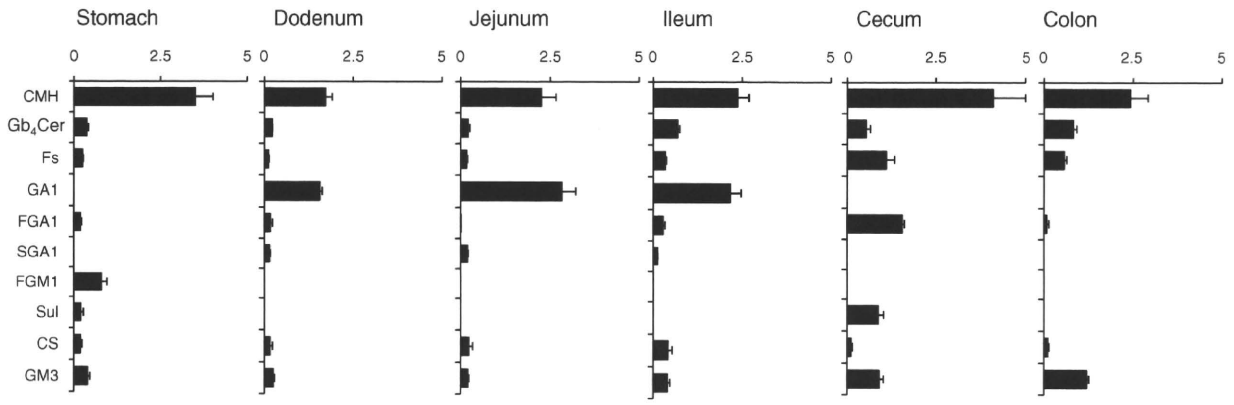

Fig. 3 Amounts of glycolipids and CS in tissues of the murine digestive tract (μg/mg dry tissue weight)

Table 1 Total amounts of epithelial glycolipids in the digestive tract of mice (HR-1, ♀, 5 months old)

		Stomach	Duodenum	Jejunum	Ileum	Cecum	Colon
Dry tissue weight (mg/mouse)		46.5±3.5	22.8±2.8	134.0±19.3	119.5±6.1	25.8±7.2	45.2±1.9
CMH	(μg/mg)	3.5±0.5	1.7±0.2	2.3±0.4	2.4±0.3	4.1±0.9	2.4±0.5
	(μg/mouse)	164.1±24.2	39.2±4.3	302.8±54.9	284.4±37.0	105.8±23.2	109.4±22.6
GA1	(μg/mg)	–	1.6±0.1	2.8±0.4	2.2±0.3	–	–
	(μg/mouse)	–	35.6±1.6	379.2±52.3	259.3±35.9	–	–
FGA1	(μg/mg)	0.19±0.04	0.17±0.06	0.01±0.00	0.28±0.05	1.56±0.06	0.08±0.06
	(μg/mouse)	8.7±1.9	3.9±1.4	1.3±1.3	33.5±6.0	40.2±1.5	3.6±2.7
SGA1	(μg/mg)	–	0.15±0.02	0.19±0.02	0.12±0.01	tr	
	(μg/mouse)	–	3.4±0.5	25.5±2.7	14.3±1.2	–	–
FGM1	(μg/mg)	0.79±0.16	–	–	–	–	–
	(μg/mouse)	36.7±7.4	–	–	–	–	
Sulfatide	(μg/mg)	0.20±0.07	–	–	–	0.88±0.15	–
	(μg/mouse)	9.3±3.3	–	–	–	22.7±3.9	–
CS	(μg/mg)	0.19±0.05	0.16±0.07	0.23±0.07	0.42±0.11	0.11±0.04	0.11±0.03
	(μg/mouse)	8.8±2.3	3.6±1.6	30.8±9.4	50.2±13.1	2.8±1.0	5.0±1.4

Values are the means of eight samples

Lactobacillus johnsonii in the cecal and colonic contents

Rabbit polyclonal anti-*Lactobacillus johnsonii* (LJ) antisera reacted with di-, tri- and tetrahexaosyl diglycerides as the major antigens in the cell wall of LJ, and also reacted with di- and trihexaosyl diglycerides in *Lactobacillus casei* (LC), but the glycolipid profiles detected on TLC-immunostaining of LJ were clearly distinct from those of LC (Fig. 8). The structures of dihexaosyl diglycerides (DH-DG) in LJ and LC were identical with each other and were determined to be as Galα1-2Glcα-DG by permethylation analysis, and enzyme treatment with α-galactosidase and α-glucosidase, as reported in the literature [19, 20]. The amounts of glycolipids in LJ were estimated to be 0.20 μg DH-DG, 0.17 μg TriH-DG and 0.22 μg TetH-DG per 1×10^8 cells, respectively. On cultivation of the cecal contents in MRS broth, followed by analysis of the bacterial glycolipids by TLC-immunostaining, the same glycolipids as those in LJ were detected in the lipid extracts of bacteria cultured under both aerobic and anaerobic conditions (lines A and N in Fig. 8). Also, when fresh cecal contents (0.01–1 μg wet weight) were cultured on a $CaCO_3$-agar GYP

Table 2 Amounts of glycolipids in contents of several regions of the digestive tract of mice (μg/mg dry wt)

	Murine Food	Gastric Contents	Jejunal Contents	Ileal Contents	Cecal Contents	Colonic Contents
Dry weight (mg/mouse)	–	12.0±1.2	7.5±1.3	16.1±4.0	65.4±1.0	85.8±0.7
Free fatty acid	0.9±0.2	16.6±0.2	8.9±0.2	1.9±0.1	0.05±0.01	0.08±0.02
Cholesterol	0.2±0.1	3.47±0.1	3.8±0.4	2.9±0.2	1.3±0.4	0.9±0.5
CS	–	0.4±0.1	0.6±0.1	0.7±0.1	0.2±0.1	0.4±0.1
Sulfatide	–	0.18±0.02	0.07±0.01	0.05±0.01	–	–
Bile acids	–	1.3±0.4	7.8±1.2	5.9±1.5	–	–
PC/PS	0.4±0.03	6.1±1.4	7.8±1.8	3.3±0.3	–	–
LPC	tr	tr	0.2±0.03	0.07±0.01	–	–
CMH	0.05±0.04	0.82±0.11	0.64±0.08	0.80±0.05	0.97±0.06	1.13±0.09
GA1	–	0.42±0.06	1.17±0.13	2.11±0.61	0.57±0.07	0.57±0.02
FGA1	–	0.05±0.02	0.04±0.01	0.06±0.02	0.02±0.01	0.02±0.01
SGA1	–	0.08±0.02	0.21±0.05	0.48±0.05	–	–
FGM1	–	0.06±0.02	0.02±0.01	0.02±0.01	–	–

Values are the means of eight samples

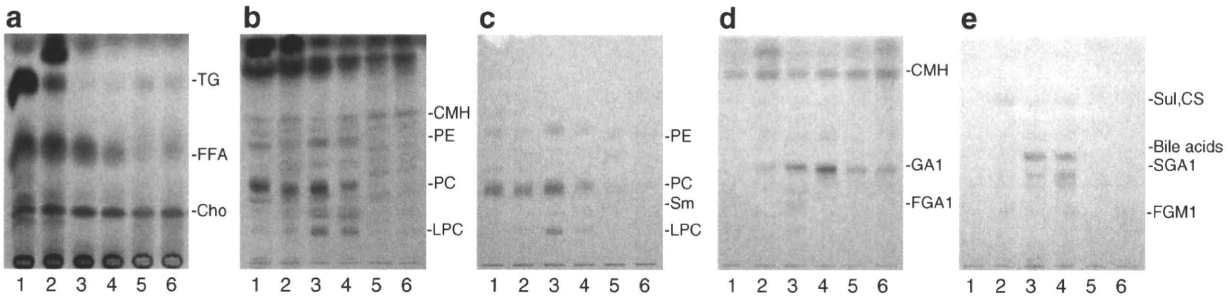

Fig. 4 TLC of lipids in the murine food and the contents of several regions of the murine digestive tract. Total lipids (**a**, **b** and **c**), and neutral (**d**) and acidic glycolipids (**e**) were developed with n-hexane/diethyl ether/acetic acid (80:30:4, by vol.) for **a**, chloroform/methanol/water (65:35:8, by vol.) for **b** and **c**, and chloroform/methanol/0.5% $CaCl_2$ in water (55:45:10, by vol.) for **d** and **e**, and were detected with cupric acetate-phosphoric acid for **a** and **b**, Dittmer's reagent for **c**, and orcinol-sulfuric acid reagent for **d** and **e**. 1, murine food; 2, stomach contents; 3, jejunal contents; 4, ileal contents; 5, cecal contents; 6, colonic contents. The lipids from the murine food, corresponding to 2 mg dry weight for **a**, **b** and **c**, and 5 mg dry weight for **d** and **e**, and those from the contents, corresponding to 0.2 mg dry weight for **a**, **b** and **c**, and 0.5 mg dry weight for **d** and **e**, were applied on a TLC-plate, respectively

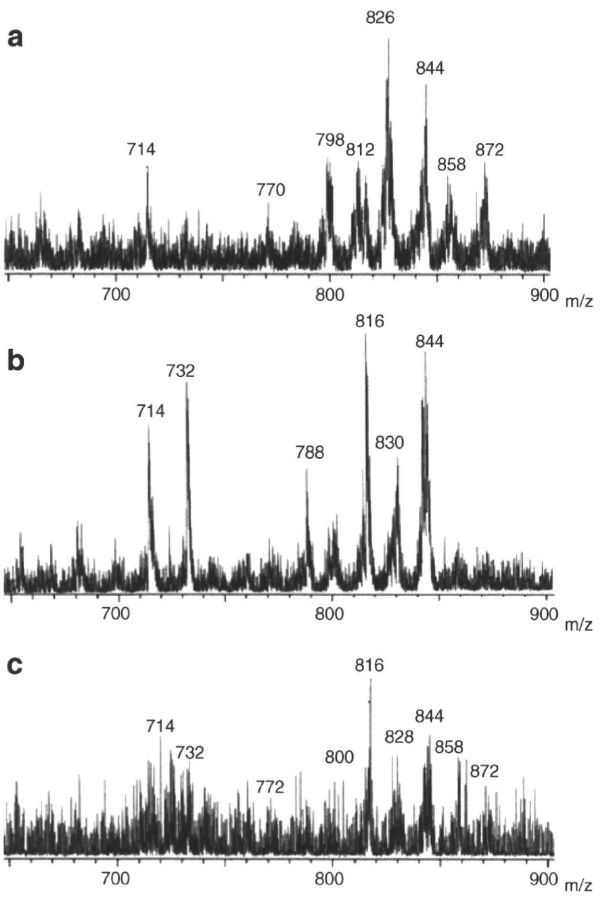

Fig. 5 Negative ion FABMS spectra of CMH from gastric tissues (**a**), jejunal tissues (**b**), and cecal contents (**c**). Triethanolamine was used as the matrix solution

plate under aerobic conditions, colonies with a clear zone, indicating the production of lactic acid, were obtained, (4.3–7.8) x 10^2 cells per μg wet weight of the contents. All colonies, less than 30 obtained at the higher dilution, were picked up with a toothpick, and their 16S-rRNA and glycolipid antigens were determined by DNA sequencing and TLC-immunostaining, respectively. As shown in Fig. 8, colonies 7 and 8 exhibited identical DNA sequences and identical glycolipid profiles to those of LJ, indicating that these colonies were certainly LJ. LJ comprised about 20% of the total colonies, the other colonies being of *Enterococcus faecalis*, and the mean number of LJ measured by colony formation was determined to be 1.1×10^6 cells per mg dry weight of the cecal contents. Then, we attempted to determine the number of LJ by direct detection of glycolipid antigens in lipid extracts of the cecal and colonic

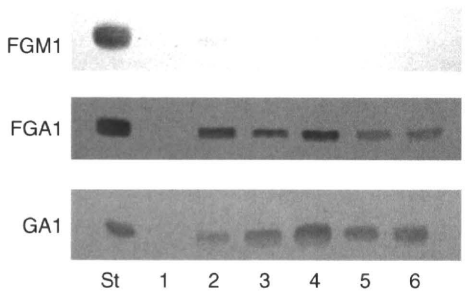

Fig. 6 TLC-immunostaining of glycolipids in the murine food and contents of several regions of the murine digestive tract. Neutral (FGA1 and GA1) and acidic(FGM1) glycolipids, corresponding to 5 mg dry weight of the murine food and 0.5 mg dry weight of the contents, were developed on plastic-coated TLC plates with chloroform/methanol /0.5% $CaCl_2$ in water (65:45:10, by vol.), and were detected with anti-FGM1, anti-FGA1 and anti-GA1 antibodies. 1, murine food; 2, stomach contents; 3, jejunal contents; 4, ileal contents; 5, cecal contents; 6, colonic contents

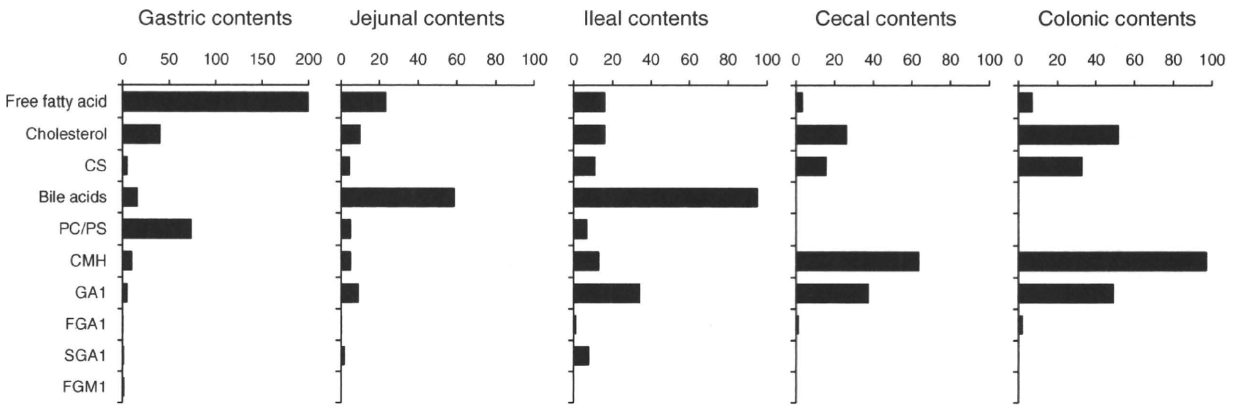

Fig. 7 Total amounts of lipids in the contents of several regions of the murine digestive tract (μg/mouse)

contents by TLC-immunostaining with anti-LJ antiserum (Fig. 9). With this procedure, the cell number as a function of the amount of glycolipids was linear from 1×10^6 to 50×10^6 cells of LJ, the limit of detection being 1×10^6 cells. On TLC-immunostaining, the cecal and colonic contents were revealed to contain 1.5×10^6 and 1.6×10^6 cells of LJ per mg dry weight, corresponding to 9.8×10^7 and 1.4×10^8 cells of LJ in the total cecal and colonic contents, respectively, which were discharged from the body together with 37 μg and 49 μg of its receptor, GA1, respectively (Fig. 7).

Discussion

As reported in this paper, sulfoglycolipids and ganglio-series glycolipids in the tissues of the murine digestive tract were found to be expressed in a region-specific manner. GA1, as the receptor, for several bacteria including lactobacilli, was preferentially expressed in the duodenum, jejunum and ileum, and its total amounts were the highest among glycolipids in these regions, amounting to 674 μg in the entire small intestine. In accord with its high amount in the small intestine, GA1 was the predominant glycolipid in the jejunal and ileal contents, comprising about 60% of the total glycolipids, probably due to the release of epithelial cells from the microvilli into the tract. Also, the relative ratios of SGA1 to GA1 in contents (14–17%) were higher than those in the tissues (4–8%), suggesting that cells containing SGA1 in relatively high amounts are readily released into the tract to give the high ratios in the contents. SGA1, GA1 and bile acids in the gastric contents were thought to be derived from the small intestine through backward flow. Similarly, since sulfatide and CS were detected in the gastro-intestinal contents at concentrations equivalent to those in the respective tissues, cells with sulfated lipids were thought to be released, to a great extent, into the tract. In contrast, Gb_4Cer and Forssman antigen in the stromal region of the villi were not detected in the contents, even in trace amounts [21].

On comparison of the lipid compositions in the contents of different regions of the digestive tract, the sites of degradation and absorption of individual lipids were clearly

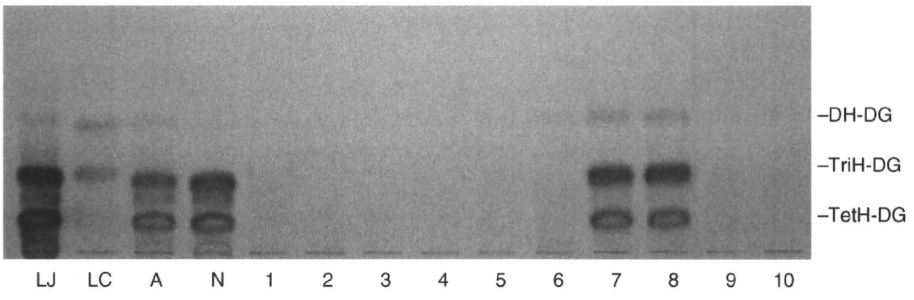

Fig. 8 TLC-immunostaining with anti-LJ antiserum of lipids from bacteria in murine cecal contents. Cecal contents (about 0.1 μg) were directly cultured in 30 ml of GYP medium under aerobic (*A*) and anaerobic (*N*) conditions at 37°C overnight, and were also cultured on $CaCO_3$-agar GYP plates under aerobic conditions, and individual colonies were cultured in 30 ml of GYP medium under aerobic conditions. The bacteria thus obtained were lyophilized, and then their lipids, corresponding to 1 mg dry weight, were developed on TLC plates with chloroform/methanol /water (65:25:4, by vol.), and were detected by TLC-immunostaining with anti-*LJ* antiserum. *LJ*, lipids from *LJ*; *LC*, lipids from *L.casei*; 1–10, lipids from bacteria in individual colonies on a $CaCO_3$-agar GYP plate

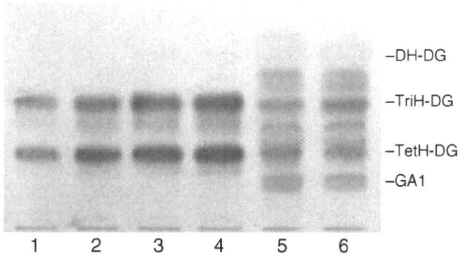

Fig. 9 TLC-immunostaining with anti-LJ antiserum of lipids from cecal and colonic contents. Lipids from LJ (1, 4.2×10^6; 2, 8.4×10^6; 3, 16.8×10^6; 4, 25.2×10^6), and the cecal (*5*) and colonic (*6*) contents, corresponding to 4 mg dry weight, were analyzed by TLC-immunostaining with anti-LJ antiserum, which also reacted with GA1 in the contents, as reported previously [5]

observed to be as follows, TG in the stomach, phospholipids in the jejunum, and free fatty acids in the ileum. The major esterified lipids in the murine food and derived from the epithelial cells, *i.e.* TG and phospholipids, and their degradation products, lysophospholipids and free fatty acids, respectively, were absent in the region between the ileum and the cecum, together with bile acids. Cholesterol, CS, GlcCer, GA1 and FGA1 became the major lipids in the cecal and colonic contents, whose lipid compositions were identical with those in feces. Since sulfatides, SGA1 and FGM1 present in the gastro-intestinal contents were not detected in the cecal and colonic contents, sulfatases and sialidases that cleave these glycolipids were present, but enzymes that cleave the glycosidic linkages in GlcCer, GA1 and FGA1 were supposed to be absent, although neutral ceramidase was reported to be present in the small intestine [22]. On the other hand, because CS sulfatase is generally insoluble in nature and is supposed not to be secreted into the digestive tract, CS was thought to be accumulated in the cecal and colonic contents [23].

As determined from the relative ion intensities of the molecular ions observed on a negative ion FABMS, about 30% of GlcCer in the cecal and colonic contents, was derived from the murine food, in which GlcCer was present at the concentration of 0.05 μg/mg dry weight, whereas GA1 and FGA1 in the cecal and colonic contents preferentially originated from the epithelial cells in the digestive tract. The total amount of GA1 in the cecal and colonic contents, a part of which was derived from SGA1, was 86 μg, corresponding to about 12% of the total GA1 in the tissues, indicating that a large amount of GA1 is excreted from the body. Since GA1 is responsible for the receptor activity toward bacteria, a possible role of GA1 in the contents was thought to be related with the discharge of bacterial flora attached to GA1. Namely, the bacterial flora attached to GA1 on intestinal epithelial cells migrates from the crypt to the villus of microvilli, and is finally liberated into the digestive tract. Even after degradation of epithelial cells during the digestion process, GA1 in the contents was supposed to remain bound to prevent the irregular spreading of bacteria in the tract. Practically, we attempted to detect LJ exhibiting binding activity toward GA1 in the cecal and colonic contents by colony formation, followed by characterization of individual colonies by sequential analysis of 16S-rRNA and detection of antigenic glycolipids with anti-LJ antisera. About 20% of the colonies obtained on cultivation of the cecal contents under aerobic conditions were shown to be LJ, amounting to 1.1×10^6 cells per mg dry weight. In addition, LJ in the cecal and colonic contents was estimated to comprise 1.5×10^6 and 1.6×10^6 cells per mg dry weight, respectively, by direct detection of antigenic glycolipids in lipid extracts with anti-LJ antiserum. The colony formation essentially indicated the living cells, whereas TLC-immunostaining indicated living, resting and dead cells, causing the difference in the cell numbers obtained with the two procedures. However, as clearly shown in Fig. 8, TLC-immunostaining with anti-LJ antiserum made it possible to detect LJ in lipid extracts of the cecal and colonic contents, indicating that it is applicable to the quantitative detection of LJ in materials stored after lyophilization, as well as fresh ones. As calculated from the average molecular weight of GA1 containing *N*-cerebronoyl phytosphingosine (1372), 37 μg of GA1 in the cecal contents represented 27 nmole, corresponding to 1.6×10^{16} molecules, which was sufficient for one-to-one binding of 9.8×10^7 cells of LJ in the cecal contents. Although anti-LJ antiserum reacted with Galα1-2Glcα1-3DG, as a common glycolipid of lactobacillus species, in our preliminary experiment, TriH-DG and TetH-DG were not detected in the ratios observed in LJ in other lactobacilli, *i.e. L. casei, L. fermentum, L. plantarum, L. ruteri* and *L. rhamnosus,* indicating that both glycolipids exhibit strong antigenicity and that anti-LJ antiserum is a useful tool for detection of symbiotic lactobacilli, *e.g.* LJ. Similarly, glycolipids characteristic of individual bacterial species can be probably detected by direct immunization with the respective bacteria.

In this connection, the strong antigenicities of DG-type glycolipids in Gram-positive bacteria and lipooligosaccharides in Gram-negative bacteria have been well recognized to be useful for the serotyping of bacterial species [13, 24], and to cause the production of natural antibodies related to blood group antigens in normal human sera [25], and of disease-related antibodies in patients suffering from multiple sclerosis [26] and Guillan-Barré syndrome [27, 28]. In addition to DG-type glycolipids, structures mimicking the oligosaccharide of GA1 were found to be present in glycoprotein of LJ, and to generate antibodies against GA1 on immunization with LJ, as shown in Fig. 9. The resemblance of the epitope structures in bacteria and a host might be essentially related with the mechanism for evading immune responses and allow LJ symbiosis in the

digestive tract, as reported previously [5]. Thus, the immune system of a host animal recognizes individual bacteria through glycolipids in the bacterial cell wall, and bacteria utilize these glycolipids in the host as receptors, indicating that cross-talk mediated by glycolipids between bacteria and the host is essential for the establishment of symbiosis.

References

1. IUPAC-IUB Commission on Biochemical Nomenclature: The Nomenclature of Lipids. Eur. J. Biochem. **179**, 11–21 (1977)
2. Karlsson, K.A.: Animal glycosphingolipids as membrane attachment sites for bacteria. Annu. Rev. Biochem. **58**, 309–350 (1989)
3. Yamamoto, K., Miwa, T., Taniguchi, H., Nagano, T., Shimamura, K., Tanaka, T., Kumagai, H.: Binding specificity of Lactobacillus to glycolipids. Biochem. Biophys. Res. Commun. **228**, 148–152 (1996)
4. Neeser, J.R., Granato, D., Rouvet, M., Servin, A., Teneberg, S., Karlsson, K.A.: Lactobacillus johnsonii La1 shares carbohydrate-binding specificities with several enteropathogenic bacteria. Glycobiology **10**, 1193–1199 (2000)
5. Iwamori, M., Shibagaki, T., Nakata, Y., Adachi, S., Nomura, T.: Distribution of receptor glycolipids for lactobacilli in the murine digestive tract and production of antibodies cross-reactive with them by immunization of rabbits with lactobacilli. J. Biochem. **146**, 185–191 (2009)
6. Lin, B., Hayashi, Y., Saito, M., Sakakibara, Y., Yanagisawa, M., Iwamori, M.: GDP-fucose: beta-galactoside alpha1, 2-fucosyltransferase, MFUT-II, and not MFUT-I or -III, is induced in a restricted region of the digestive tract of germ-free mice by host-microbe interactions and cycloheximide. Biochim. Biophys. Acta **1487**, 275–285 (2000)
7. Bry, L., Falk, P.G., Midtvedt, T., Gordon, J.I.: A model of host-microbial interactions in an open mammalian ecosystem. Science **273**, 1380–1383 (1996)
8. Iwamori, M., Domino, S.E.: Tissue-specific loss of fucosylated glycolipids in mice with targeted deletion of α(1, 2)fucosyltransferase genes. Biochem. J. **380**, 75–81 (2004)
9. Yoneshige, A., Sasaki, A., Miyazaki, M., Kojima, N., Suzuki, A., Matsuda, J.: Developmental changes in glycolipids and synchronized expression of nutrient transporters in the mouse small intestine. J. Nutr. Biochem. **21**, 214–226 (2010)
10. Gustafsson, B.E., Karlsson, K.A., Larson, G., Midtvedt, T., Strömberg, N., Teneberg, S., Thurin, J.: Glycosphingolipid patterns of the gastrointestinal tract and feces of germ-free and conventional rats. J. Biol. Chem. **261**, 15294–15300 (1986)
11. Larson, G., Watsfeldt, P., Falk, P., Leffler, H., Koprowski, H.: Fecal excretion of intestinal glycosphingolipids by newborns and young children. FEBS Lett. **214**, 41–44 (1987)
12. Larson, G., Falk, P., Hoskins, L.C.: Degradation of human intestinal glycosphingolipids by extracellular glycosidases from mucin-degrading bacteria of the human fecal flora. J. Biol. Chem. **263**, 10790–10798 (1988)
13. Manual of microbiological culture media, Difco & BBL Manual, Becton, Dickinson and Company, Sparks, MD, USA (2003)
14. Iwamori, M., Ohta, Y., Uchida, Y., Tsukada, Y.: *Arthrobacter ureafaciens* sialidase isoenzymes, L, M1 and M2, cleave fucosyl GM1. Glycoconj. J. **14**, 67–73 (1997)
15. Iwamori, M., Kaido, T., Iwamori, Y., Ohta, Y., Tsukamoto, K., Kozaki, S.: Involvement of the C-terminal tail of Arthrobacter ureafaciens sialidase isoenzyme M in cleavage of the internal sialic acid of ganglioside GM1. J. Biochem. **138**, 327–334 (2005)
16. Iwamori, M., Takamizawa, K., Momoeda, M., Iwamori, Y., Taketani, Y.: Gangliosides in human, cow and goat milk, and their abilities as to neutralization of cholera toxin and botulinum type A neurotoxin. Glycoconj. J. **25**, 675–683 (2008)
17. Woese, C.R., Kandler, O., Wheelis, M.L.: Towards a natural system of organisms: proposal for the domains Archaea, Bacteria, and Eucarya. Proc. Natl Acad. Sci. USA **87**, 4576–4579 (1990)
18. Leffler, H., Hansson, G.C., Strömberg, N.: A novel sulfoglycosphingolipid of mouse small intestine, IV3-sulfogangliotetraosylceramide, demonstrated by negative ion fast atom bombardment mass spectrometry. J. Biol. Chem. **261**, 1440–1444 (1986)
19. Shaw, N.: Bacterial glycolipids. Bacteriol. Rev. **34**, 365–377 (1970)
20. Shaw, N., Baddiley, J.: Structure and distribution of glycosyl diglycerides in bacteria. Nature **217**, 142–144 (1970)
21. Suzuki, A., Yamakawa, T.: The different distributions of asialo GM1 and Forssman antigen in the small intestine of mouse demonstrated by immunofluorescence staining. J. Biochem. **90**, 1541–1544 (1981)
22. Kono, M., Dreier, J.L., Ellis, J.M., Allende, M.L., Kalkofen, D.N., Sanders, K.M., Bielawski, J., Bielawska, A., Hannun, Y.A., Proia, R.L.: Neutral ceramidase encoded by the Asah2 gene is essential for the intestinal degradation of sphingolipids. J. Biol. Chem. **281**, 7324–7331 (2006)
23. Cui, Y., Iwamori, M.: Distribution of cholesterol sulfate and its anabolic and catabolic enzymes in various rabbit tissues. Lipids **32**, 599–604 (1997)
24. Sugiyama, T., Smith, P.F., Langworthy, T.A., Mayberry, W.R.: Immunological analysis of glycolipids and lipopolysaccharides derived from various mycoplasmas. Infect. Immun. **10**, 1273–1279 (1974)
25. Alving, C.R., Fowble, J.W., Joseph, K.C.: Comparative properties of four galactosyl lipids as antigens in liposomes. Immunochemistry **11**, 475–481 (1974)
26. Hirsch, H.E., Parks, M.E.: Serological reactions against glycolipid-sensitized liposomes in multiple sclerosis. Nature **264**, 785–787 (1976)
27. Jacobs, B.C., Rothbarth, P.H., van der Meché, F.G., Herbrink, P., Schmitz, P.I., de Klerk, M.A., van Doorn, P.A.: The spectrum of antecedent infections in Guillain-Barré syndrome: a case-control study. Neurology **51**, 1110–1115 (1998)
28. Houliston, R.S., Yuki, N., Hirama, T., Khieu, N.H., Brisson, J.R., Gilbert, M., Jarrell, H.C.: Recognition characteristics of monoclonal antibodies that are cross-reactive with gangliosides and lipooligosaccharide from Campylobacter jejuni strains associated with Guillain-Barré and Fisher syndromes. Biochemistry **46**, 36–44 (2007)

balt5/zhl-hp/zhl-hp/zhl00311/zhl5567-11z | xppws | S=1 | 12/31/10 | 5:08 | Art: 200345 | Input-9000

Health Physics., 100: 266-268, 2011

Abstract

BIOLOGICAL CONSEQUENCES AND HEALTH CONCERNS FROM LOW-DOSE AND LOW-DOSE-RATE RADIATION IN MICE AND HUMANS

Taisei Nomura*

Fn1 Dose and dose-rate effectiveness are among the most important ways to estimate the risk of low-level radiation exposure to humans. This is important because humans have been exposed continuously to low and low dose-rate radiation for a long time. However, there is a scarcity of information about low dose-rate exposure in humans, even though abundant human data (more than animal data) are available from populations accidentally exposed to high doses of radiation at high dose-rates, including atomic bomb survivors and patients undergoing medical treatment. If radiation damage by very low doses of radiation is completely repaired, there is no accumulation of DNA damage resulting in no increase of cancer and other defects; i.e., "threshold." Consequently, DDREF (dose and dose rate effectiveness factor) is an important factor to estimate low-level radiation exposure to humans. Radiation effects are also influenced or modified by the environment and intrinsic bio-defense systems, such as immune surveillance and programmed cell death. In this paper, dose and dose rate effectiveness are discussed, based on published and unpublished data for mice and humans, to resolve underlying problems for the evaluation of the health risks of low-level exposure to ionizing radiation. Discussion will include the effects of neutrons.

About 80% of fatal radiation risk derives from cancer. Large-scale animal experiments were carried out in the U.S., Europe, and Japan in which young adult animals were irradiated at either high dose rates using x- or γ-rays for a few minutes, or at low dose rates continuously for long periods, usually over a lifetime (IARC 2000). Considering the age-dependent cancer sensitivity and latent period for cancer induction, the animals had to be irradiated during the same period at different dose rates for precise DDREF estimation. Otherwise, most radiation doses were given at older ages (less cancer-sensitive stages) and just after the tumor occurrence or before death . It was also necessary to use more than two different strains of animals to simulate various types of tumors found in humans. In these experiments, for example, two strains of mice (C57BL/6J and C3H/HeJ) were exposed to γ-rays at 6, 7, 8, and 9 wk of age at seven different dose rates (0.04 to 570 mGy min^{-1}). Dose rate effects were not apparent in solid tumors at medium (0.5 Gy) and high doses (1.7 Gy). High incidence of tumors in radiation-sensitive organs such as ovaries in mice concealed dose rate effects in other organs, while there were apparent dose rate effects for the induction of leukemia and skin tumors. In the lower dose (total dose 0.1 Gy × 4) and low dose rate (0.04 mGy min^{-1}) experiment, however, large and significant dose rate effects were observed in various solid tumors (DDREF; 2 to 4) at low dose rate exposure. Thus, dose rate effects were essential and dose- and age-dependent, and values of DDREF were organ-dependent (Nomura 1998, 2002; Nomura et al. in preparation). AQ: A However, such dose rate effects were not observed in double-strand break repair deficient SCID (severe combined immunodeficient) mice (Nomura 1998), suggesting that dose rate effect was caused by the recovery capability of mouse tissues for the most part. AQ: B

Low dose rate exposure to x-rays (4.3 mGy min^{-1}) reduced somatic (embryonic) mutations (and also cancer) at specific loci to one third of those induced by high dose rate (540 mGy min^{-1}) exposure, showing a similar level of dose rate effect to the germ line mutations (Nomura et al. 1990; Nomura 1998, 2002). Significant reduction of congenital malformation (1/20) was also observed by low dose rate exposure (4.3 mGy min^{-1}) in wild mice, but not in SCID mice.

Dose rate effects were observed in radiation induced germ-line mutations. Mouse specific locus mutations indicated apparent dose rate effects in the offspring of

* National Institute of Biomedical Innovation and Osaka University, 7-6-8 Saito Asagi, Ibaraki, Osaka 567-0085, Japan.

For correspondence contact the author at the above address, or email at n5nomura@nibio.go.jp.

(*Manuscript accepted* 25 *May* 2010)

0017-9078/10/0

DOI: 10.1097/HP.0b013e3181e9b10d

balt5/zhl-hp/zhl-hp/zhl00311/zhl5567-11z | xppws | S=1 | 12/31/10 | 5:08 | Art: 200345 | Input-9000

mice irradiated at the stages of spermatogonia (DDREF, about 3) and oocytes (about 20). Similar results were obtained in transgenerational carcinogenesis in mice by fractionated irradiation of parental mice (Nomura 1982, 2006). Tumor incidence in F_1 offspring increased after parental exposure to x-rays (single dose); however, there were no increases of tumors in the offspring by fractionated irradiation (0.36 Gy, 2 h apart) of spermatogonia and oocytes. Such dose fractionation effects were not observed by the post-meiotic exposure (Nomura 1982).

To confirm dose rate effects and also tumor enhancement by postnatal environments, male N5 mice were exposed to 2.16 Gy of γ-rays at spermatoginia stages and tumor promoter TPA was given postnatally to their F_1 offspring (6 wk after birth). Significant increases of skin cancer and leukemia were observed in the offspring after preconceptional irradiation at a high dose rate (570 mGy min^{-1}) coupled with TPA post-treatments. However, there were no increases of skin cancer and leukemia after low dose rate exposure (0.2 mGy min^{-1}) coupled with TPA post-treatments, showing high DDREF (8.7 and 4.8, respectively) (Nomura et al. in
AQ: C preparation). Similar findings were also observed in skin cancer and hepatoma after in utero exposure to x- rays, γ-rays, and ^{252}Cf neutrons coupled with TPA or phenobarbital post-treatments (Nomura 1998; Nomura et al. 1990). Initial events using in utero or germ-line irradiation had to be memorized in the embryonic cells and germ cells and caused tumors, as shown by the post-treatments with promoting agents (Nomura 1983, 2003, 2006; Nomura et al. 1990, 2004). Postnatal environments may be important in radiation carcinogenesis in humans who have more chances to be exposed to various carcinogenic/promoting agents in the diet and environment in contrast to mice reared under specified conditions. Recent studies with microarray technology revealed that germ-line exposure to radiation induced changes in gene expression of biochemical, physiological and immunological functions in the progeny. Accumulation of these changes may enhance tumor incidence in the next generation (Nomura 2003, 2006, 2008; Nomura et al. 2004).

Currently, the author is examining microsatellite mutations and cancer in the offspring of N5 male mice exposed to 0.1 to 0.6 Gy of fission neutrons from the nuclear reactor UTR-KINKI. Significant increases in microsatellite mutations and leukemia are observed in the offspring after 0.2 Gy and higher doses of neutron exposure (Ryo and
AQ: D Nomura et al. in preparation). However, such increases have not yet been found in microsatellite mutations in the children of liquidators in Chernobyl (Furitsu et al. 2005) and atomic bomb survivors in Hiroshima/Nagasaki (Kodaira et al. 2010). One research group reported increases of minisatellite mutations in the children of inhabitants of Chernobyl, Semipalatinsk, and Techa River, but other groups have not found such increases in the children of the liquidators in Chernobyl and atomic bomb survivors (Nomura 2009).

A novel experimental system was established to maintain morphology and function of normal human organs and tissues in the improved SCID mice for several years (Nomura et al. 1997, 2008; Fukuda et al. 1998). Human skin and thyroid tissues maintained in the improved SCID mice were exposed to daily doses of UVB-light, or weekly doses of x-rays or ^{137}Cs γ-rays for a period of approximately 2 y. It was reported that among 18 normal skins exposed to doses of 73 to 180 J cm^{-2}, 14 actinic keratoses (77.8%) and 3 squamous cell carcinomas (16.7%) developed, whereas neither actinic keratosis nor cancer was observed in 15 human skins not exposed to UVB (Nomura et al. 1997).

Consecutive exposure of normal thyroid gland tissues from the head and neck of cancer patients (average of 60 y old) or human thyroid glands from young Graves' disease patients (20 y old) induced morphological changes (disappearance of follicles, necrosis, etc.) and a decrease in thyroid hormone secretion with increasing doses of γ-rays at high dose rate (1,189 mGy min^{-1}), whereas no substantial changes were observed in thyroid tissues exposed to the same doses at low dose rate (0.23 mGy min^{-1}) (Nomura et al. 2008). Significant increases in *p53* and *c-kit* mutation were detected in transplanted thyroid tissues exposed to cumulative doses of 8–33 Gy at high dose rate. However, no mutations were detected in thyroid tissues whether or not they were exposed to the low dose rate γ-rays, showing an apparent dose rate effect. Thus, human tissues exhibit a strong ability to AQ: E recover from radiation damage.

Fission neutrons from the nuclear reactor UTR-KINKI induced similar morphological changes in human thyroid tissues, and reduction of thyroid hormone secretion by fission neutrons suggested high relative biological effectiveness (RBE, 6.5) in comparison with x-rays and ^{137}Cs γ-rays (Adachi et al. 2010). Microarray analyses revealed dose-dependent changes in gene expression against unexposed concurrent controls with increasing doses of fission neutrons (0.2 to 0.6 Gy) and ^{137}Cs γ-rays (1.0 to 3.0 Gy) and showed high RBE (4.2). Furthermore, there were 14 specific genes that showed more than 4-fold change in gene expression in all the thyroid tissues exposed to higher doses of radiation, especially neutrons (0.4 and 0.6 Gy), but none at lower doses (0.2 Gy of neutrons and 1.0 and 2.0 Gy of γ rays). Eight of them were related to genes responding to injury or stress, three were related to apoptosis, and two were related to transcription. This is the first experimental

report that fission neutrons can induce some morphological and functional disorders in human tissues, showing high RBE against γ-ray exposure. Health Phys. 100(3):000–000; 2011

Key words: cancer; genetic effects; radiation effects; radiation, low-level

Acknowledgments—This work is supported by the Grants-in-Aid for Scientific Research (MEXT and MHLW, Japan), by the Research for the Future (JSPS), and by the Japan Space Forum.

REFERENCES

Adachi S, Ryo H, Hongyo T, Nakajima H, Tsuboi-Kikuya R, Tokita Y, Matsuzuka F, Hiramatsu K, Fujikawa K, Itoh T, Nomura T. Effects of fission neutrons on human thyroid tissues maintained in SCID mice. Mutat Res 696:107–113; 2010.

Fukuda K, Nakajima H, Taniguchi E, Sutoh K, Wang H, Hande PM, Li LY, Kurooka M, Mori K, Hongyo T, Kubo T, Nomura T. Morphology and function of human benign tumors and normal thyroid tissues maintained in severe combined immunodeficient mice. Cancer Letters 132:153–158; 1998.

Furitsu K, Ryo H, Yeliseeva KG, Thuy LTT, Kawabata H, Krupnova EV, Trusova VD, Rzheutsky VA, Nakajima H, Kartel N, Nomura T. Microsatellite mutations show no increases in the children of the Chernobyl liquidators. Mutat Res 581:69–82; 2005.

IARC. IARC monograph on the evaluation of carcinogenic risks to humans. Vol. 75: Physical Agents: Ionizing radiation, Part I, x-rays, γ-rays and neutrons. Lyon: IARC; 2000.

Kodaira M, Ryo H, Kamada H, Furukawa K, Takahashi N, Nakajima H, Nomura T, Nakamura N. No evidence of increased mutation rates at microsatellite loci in offspring of A-bomb survivors. Radiat Res 173:205–213; 2010.

Nomura T. Parental exposure to x- rays and chemicals induces heritable tumours and anomalies in mice. Nature 296:575–577; 1982.

Nomura T. X-ray induced germ-line mutation leading to tumors; its manifestation in mice given urethane postnatally. Mutat Res 121:59–65; 1983.

Nomura T. Dose rate effectiveness and repair in radiation-induced mutagenesis, teratogenesis, and carcinogenesis in mice. In: Sharan RN, ed. Trends in radiation and cancer biology. Julich, Germany: Forschungzentrum; 1998: 149–155.

Nomura T. Dose and dose rate effect in mutagenesis, teratogenesis and carcinogenesis. In: Sugahara, ed. Radiation and homeostasis. Amsterdam: Elsevier Science; 2002: 105–110.

Nomura T. Transgenerational carcinogenesis: Induction and transmission of genetic alterations and mechanisms of carcinogenesis. Mutat Res 544:425–432; 2003.

Nomura T. Transgenerational effects of radiation and chemicals in mice and humans. J. Radiat Res 47:(Suppl B):83–97; 2006.

Nomura T. Transgenerational effects from exposure to environmental toxic substance. Mutat Res Rev 659:185–193; 2008.

Nomura T. Transgenerational health concerns from radiation in mice and humans. In: The 15th Alexander Hollaender Course, Astana. 2009. AQ: F

Nomura T, Nakajima H, Hatanaka T, Kinuta M, Hongyo T. Embryonic mutation as a possible cause of in utero carcinogenesis in mice revealed by postnatal treatment with 12-0-tetradecanoylphorbol-13-acetate. Cancer Res 50:2135–2138; 1990.

Nomura T, Nakajima H, Hongyo T, Taniguchi E, Fukuda K, Li YL, Kurooka M, Sutoh K, Hande TM, Kawaguchi T, Ueda M, Takatera T. Induction of cancer, actinic keratosis and specific p53 mutations by ultraviolet light B in human skin maintained in SCID mice. Cancer Res 57:2081–2084; 1997.

Nomura T, Nakajima H, Ryo H, Li LY, Fukudome Y, Adachi S, Gotoh H, Tanaka H. Transgenerational transmission of radiation- and chemically-induced tumors and congenital anomalies in mice: studies of their possible relationship to induced chromosomal and molecular changes. Cytogenet Genome Res 104:252–260; 2004.

Nomura T, Hongyo T, Nakajima H, Li LY, Syaifudin M, Adachi S, Ryo H, Baskar R, Fukuda K, Oka Y, Sugiyama H, Matsuzuka F. Differential radiation sensitivity to morphological, functional and molecular changes of human thyroid tissues and bone marrow cells maintained in SCID mice. Mutat Res 657:68–76; 2008.

■ ■

JOBNAME: AUTHOR QUERIES PAGE: 1 SESS: 1 OUTPUT: Fri Dec 31 05:08:58 2010
/balt5/zhl-hp/zhl-hp/zhl00311/zhl5567-11z

AUTHOR QUERIES

AUTHOR PLEASE ANSWER ALL QUERIES 1

A—Update Nomura et al in preparation. If not in print or in press, move to footnote as unpublished. If in print or in press, add complete citation to reference list.

B—Is this change OK?

C—Update Nomura et al. in preparation.

D—Update Ryo and Nomura et al in preparation. If not in print or in press, move to footnote as unpublished. If in print or in press, add complete citation to reference list.

E—Is this change OK?

F—Add complete publication info to Nomura 2009.

宇宙環境の人体影響評価と防護に関する研究

医薬基盤研究所: 野村 大成、梁 治子、足立 成基、時田 偉子, 堀家 なな緒、畑中 英子、
菊谷 理絵
阪大医: 中島 裕夫、本行 忠志、
近大理工/原研: 藤川 和男、伊藤 哲夫、
三菱重工: 落合 俊昌, 行徳 淳一郎,
アミノアップ化学: 若命 浩二

Evaluation of Human Risk in Space Environment and Its Protection

Taisei Nomura, Haruko Ryo, Shigeki Adachi, Yoriko Tokita, Nanao Horike, Eiko Hatanaka, Rie Kikuya, National Institute of Biomedical Innovation, Ibaraki, Osaka 567-0085
Hiroo Nakajima, Tadashi Hongyo, Graduate School of Medicine, Osaka University, Suita, Osaka 565-0871,
Kazuo Fujikawa, Tetsuo Itoh, Atomic Energy Research Institute, Kinki University, Higashiosaka, Osaka 577-8502
Toshimasa Ochiai, Junichiro Gyotoku, Mitsubishi Heavy Industry, Kobe, Hyogo 652-8585
Kouji Wakame, Amino up Chemical, Sapporo, Hokkaido 004-0839
E-Mail: n5nomura@nibio.go.jp

Abstract: To study the human risk of cosmic environment (including neutrons) in the flying body and space base, (1) Morphological and functional effects (including changes in gene expression) of fission neutrons on human thyroid tissues maintained in super-SCID (severe combined immunodeficient) mice, (2) Microsatellite mutations and leukemia in the offspring of mice in the space environment, and (3) Protection of radiation-induced defects by food and supplement, and effects of space environment (including micro-gravity) on human diseases are carried out by using specific mouse models. The first two projects are ready to be carried out in the space environment, although these were cancelled in Japan (and also in USA and EU). As for Project 3, we demonstrated protection of leukemia and congenital anomalies by AHCC (Active Hexose Correlated Compound) treatment, and strong effects of micro-gravity (μG) on behavior and gene expression by parabolic flight were shown with panic mouse model.

Key words; Space Environment, Cosmic Radiations, Human Risk, Super-SCID-Human Mice, Transgenerational Effects, Parabolic Flight, Cancer Prevention, Behavior, Changes in Gene Expression

人類は、将来、宇宙生活の必要性に迫られることが考えられ、最先端かつ安全な宇宙飛行技術の開発とともに、人類が宇宙生活を行うにあたり不可欠なのが、宇宙環境および宇宙放射線（宇宙基地、飛翔体内のヒト被曝の主たる放射線である中性子線）による人体影響、即ち、重力変化等の生体影響や忘れた頃に頭をもたげてくるがんや生活習慣病の防御である。宇宙環境（含、宇宙放射線）による人体影響の評価と防護研究のため、「宇宙環境の人体影響評価と防護に関する研究」研究チームでは、20年間にわたり、

1）SCIDプロジェクト：ヒト臓器・組織機能を数年にわたり継代維持できる超重度複合免疫不全マウス（super-SCIDマウス）を用いたヒト組織の形態、機能、遺伝子変異、遺伝子発現への影響研究、
2）継世代プロジェクト：宇宙放射線等宇宙環境の子孫におよぼす影響、特に、がん、突然変異、発生異常の検出、
3）宇宙創薬プロジェクト：がん等各種生活習慣病、情動行動異常等自然発症モデルマウスや安全性高感度検出モデルマウスを用いた宇宙環境（含、宇宙放射線）に対する生体反応と防護に関する研究を行っている。

これら研究は、我が国独自の発見、開発によるものであり、人類が宇宙環境利用、あるいは、宇宙環境で生活するためには避けて通れない研究課題であり、宇宙生活や宇宙よりの帰還後を想定した基盤研究を行ってきた。現在、哺乳動物個体の打ち上げ実験は中断しているが、いつでも宇宙実験が出来るよう常備体制を維持している。

上記 3 本柱の内、3 番目の疾患モデルマウスを用いた宇宙医学（創薬）研究に関しては、食品やサプリメントによる放射線誘発がん等の発生の防護に関する研究など、地上での防護実験も可能であり、重力変化に対する生体反応に関する研究においては、パラボリックフライトでも一部目的が達せられる。そのため、医薬基盤研究所の野村プロジェクト特有のモデルマウスを用いパラボリックフライト（μG）による行動異常と遺伝子発現の変化に関する共同研究を行っている。

2010 年度の成果を紹介する。

1．ヒト臓器・組織置換マウス等を用いた宇宙環境の人体影響研究（SCID プロジェクト）

宇宙環境、宇宙放射線の人体影響を想定した地上実験を計画するにあたり用意したヒト甲状腺組織置換超重度複合免疫不全マウス（super-SCID マウス）は、環境変化の人体影響を少数例で高感度に検出できる日本発、世界初の人体影響評価システムである。通常の宇宙実験はヒトが動物、細胞等を宇宙に運ぶが、本実験では、マウスがヒト組織をおんぶして運ぶことになる。平成 22 年度には以下の成果が得られている。

1）ヒト甲状腺組織に対する中性子線の形態・機能への影響

宇宙放射線類似線源（近畿大学研究用原子炉 UTR-KINKI 中性子線 0.2 Gy/h とγ線 0.2 Gy/h）による、ヒト甲状腺組織の濾胞の消失と壊死、機能低下（ヒト甲状腺ホルモンの分泌能低下、RBE 値 6.5）が示された（Mutat. Res., 2010, Space Utiliz. Res., 2010）。

2）遺伝子発現の変化

中性子線照射を受けた甲状腺組織において 4 倍以上の遺伝子発現の変化を示す遺伝子数が線量依存的に増加した（RBE：4.2）（Fig. 1）。

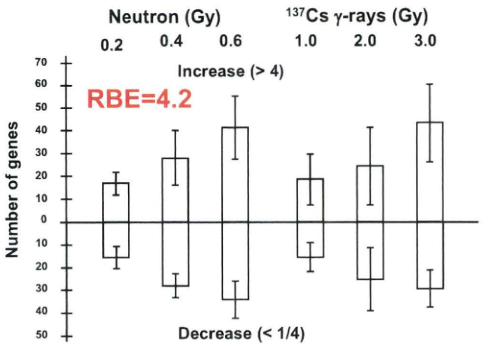

Fig. 1. Dose-dependent changes in gene expression in the transplanted human thyroid tissues after neutron and γ-ray exposures (Mutat Res, 2010).

しかも、照射を受けた全てのヒト甲状腺組織において、4 倍以上の遺伝子発現の変化を示す特定の遺伝子 14 個を発見した（ストレス、損傷、アポトーシス及び転写に関与する遺伝子）（Mutat Res, 2010）（Table 1）。

14 Genes Responding to Radiations

C7orf68	+chromosome 7 open reading frame 68
SERPINE1	+serpin peptidase inhibitor, clade E (nexin)
ADM	+adrenomedullin
ENO2	+enolase 2
ANGPTL4	+angiopoietin-like 4
PLIN2	+perilipin 2
DIO1	- deiodinase, iodothyronine
COL9A3	- collagen, type IX
TFF3	- trefoil factor
HK2	+hexokinase 2
BNIP3	+BCL2/adenovirus E1B 19kDa interacting protein
BHLHE40	+basic helix-loop-helix family
CEBPD	+CCAAT/enhancer binding protein (C/EBP)
SEMA3G	- sema domain, immunoglobulin domain

Stress and Injury; 8 genes, Apoptosis; 3 genes, Translation; 2 genes, , , ,

Table 1. 14 Genes showing more than 4-fold changes in gene expression in all the thyroid tissues exposed to fission neutrons and γ-rays. (Mutat Res, 2010)

3）ヒト臓器組織置換 Super-SCID マウスを維持し、宇宙実験にいつでも対応できるようにしている。

2．宇宙環境の次世代に及ぼす影響（継世代プロジェクト）

宇宙での長期滞在計画で考慮しなければならないのは宇宙環境の子孫に及ぼす影響である。遺伝影響（継世代影響）は、40 年間続けてきた野村のライフワークである。放射線や化学物質が親マウスに作用すると、次世代に突然変異だけでなく、ヒトによくみられるがん、形態異常、生活習慣病も発生する。

1）原子炉放射線（中性子線 0.2 Gy/h、γ線 0.2 Gy/h）の精原細胞期照射による線量依存性のマイクロサテライト突然変異の誘発、白血病の有意な増加が認められた（Fig. 2）。

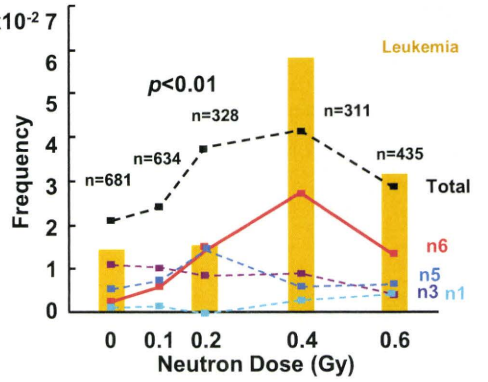

Fig. 2. Microsatellite mutation and leukemia in the progeny of N5 mice exposed to fission neutron (in preparation).

近大原子炉放射線（0.1 Gy 中性子線）を精原細胞期照射した N5♂マウスの F_1 に生後 6 週より 0.05 % フェノバルビタールを 12 ヶ月まで経口投与したところ、ヘパトーマの高騰が認められた（♀マウスで約 9 倍、♂マウスで約 2 倍；中間結果）。

3）本計画は、少数（5〜10 匹）の N5 マウス雄を宇宙に上げ、帰還後被曝雄マウスと正常雌マウスを交配することにより、数百〜数千匹の F_1 マウスを得ることが出来、発がん、突然変異等を検出することが可能なことを示しており、何時でも宇宙実験を実施できるよう準備できている。

3．疾患モデルマウスを用いた研究（宇宙創薬プロジェクト）

1）放射線誘発障害（がん、発生異常等）の防護に関する研究

放射線誘発がん等に対する食品やサプリメントによる発生の防護に関する研究を行った。

（1）放射線誘発高白血病モデルマウスに ^{137}Cs ガンマ線を照射し、2%AHCC（Active Hexose Correlated Compound：担子菌菌糸体培養抽出物）水溶液を連続経口投与することにより、白血病発生の防護のための地上研究を行い、有意な抑制効果を確認した（Figs. 3, 4, Table 2）。

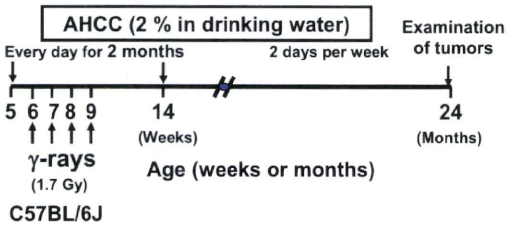

Fig. 3. Scheme of experimental procedures of AHCC treatment to C57BL/6J mice exposed to γ-rays.

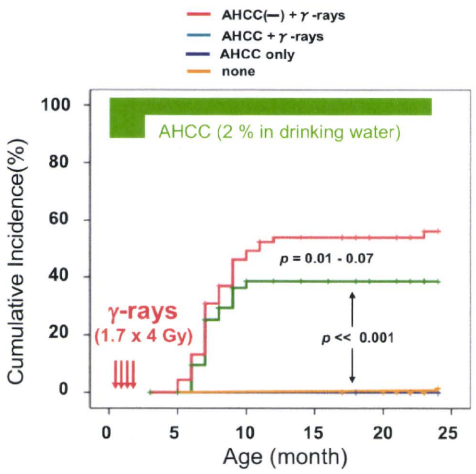

Fig. 4. Suppressive effects of AHCC on incidence of leukemia after ^{137}Cs γ-ray exposure (1.7 Gy x 4).

AHCC in Drinking water	γ-rays (Dose)	No. of mice	TBA (%)	Leukemia (%)
2 %	1.7 Gy x 4	54	29 (53.7)*	19 (35.2)*
0 %	1.7 Gy x 4	68	49 (72.1)	37 (54.4)
0 %	none	71	17 (23.9)	0 (0.0)
2 %	none	20	3 (15.0)	0 (0.0)

- 1.7 Gy of ^{137}Cs γ-rays were given 4 times at 6, 7, 8 and 9 weeks after birth.
- 2% of AHCC were given orally at 5 weeks after birth for 2 months and then 2 days per week until the end of experiment (24 months)

* $P < 0.05$ by χ^2 test

Table 2. Reduction of radiation-induced tumors and leukemia by AHCC in C57BL/6J mice

（2）重力変化や放射線・化学物質により発生異常が誘発されることは哺乳動物においても良く知られている。妊娠マウスにガンマ線を照射することにより誘発される発生異常も、Pyran、BCG 等マクロファージ活性化物質同様に（J Exp Med, 1990）、AHCC の前投与により協力に抑制されることを確認した。

2）重力変化による行動異常と遺伝子発現の変化

重力等宇宙環境の変化については、かなりの部分がパラボリックフライト等で代用できる。2009 年 12 月 17 日に、三菱重工との共同研究のひとつとして、モデルマウスの中から「パニックになりやすいマウス BH-4」を選び、パラボリックフライト（μG）実験を行った。時田偉子、行徳淳一郎が搭乗した。今回のパラボリックフライトでは、対照としてもっともおとなしいマウス BH-8 を選んだ。基礎実験では、BH-4 マウスは尾を小さなクリップで挟むと、慌てふためいて噛み切るのに対し、BH-8 マウスは平気である。両系統のマウスを 1 匹ずつケージに入れ、飛行中ビデオ撮影を行った。また、パラボリックフライト直前と直後にマウス脳等臓器を採取し、マイクロアレイを用い、遺伝子発現の 2 系統間の差、同一系統での微少重力による差を解析した（Fig. 5）。

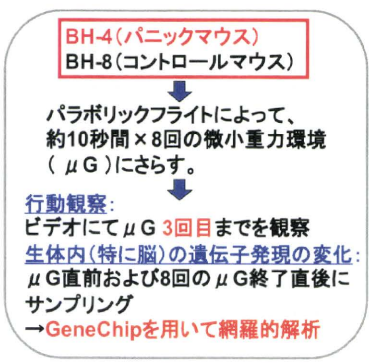

Fig. 5. Experimental procedures.

（1）パラボリックフライトにより、以下に示すごとく、行動の変化が認められた。

（i）すくみ（不安指標）：ケージ壁際へのすくみはBH-4マウスに多い。その時間（約10倍）と回数（約3倍）は、「パニックになりやすいマウス系統」の方が圧倒的に多く、大きな差がでた。

（ii）あるきまわる・うろたえる（パニックの指標）：μG終了直後、距離・時間と共にBH-4マウスに多い。BH-8はμGの回数を重ねる毎にうろつくことが少なくなった（慣れ）。しかし、BH-4マウスは、うろつく距離があり、上下運動〔立ち上がり〕もみられ、非常にパニックな様子を示した。

（iii）洗顔・毛づくろい（落ち着きの指標）：μG前だけに見られた洗顔や毛づくろいは、BH-4、BH-8マウスともにμG後は一度も無かった。平行飛行時だけを見ると、BH-4マウスは時間を追うごとに落ち着きがなくなるのに対し、BH-8マウスは逆に平行飛行が続くにしたがって落ち着く様子を見せた（Fig. 6）。

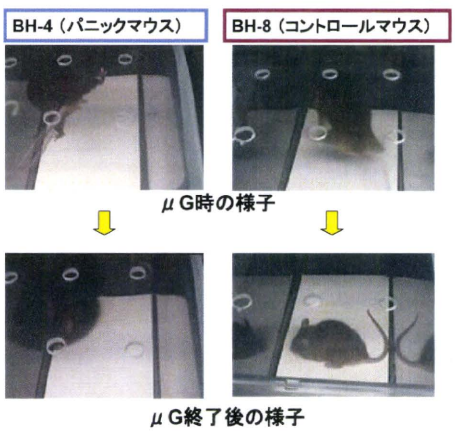

Fig. 6. Belabor before and after μG.

（2）パラボリックフライトによって遺伝子発現が変化した遺伝子数（15,000遺伝子中、大脳および小脳での16倍以上の変化）に関しては、BH-4マウスでは大脳において多くの遺伝子の発現抑制がみられたのに対し、対照に用いたBH-8マウスでは運動に関与する小脳で、非常に多くの遺伝子に発現抑制が強度に認められた。しかし、肝臓ではμG前後で大きな変化が認められなかった。瞬時の重力変化直後の生体反応が分子レベルで強烈であり、遺伝子発現の変化は脳組織特異的に起こっていると思われる（Table 3）。

また、情動行動に関与する遺伝子の変化よりも、通常の機能遺伝子の強力な発現抑制が広く見られた。さらにn数を増やし、経時的変化、ヒト組織での検出も含め、パラボリックフライト実験を2010年10月に実施、現在解析中である。

基礎実験では、BH-4マウスの行動異常は、ある種の薬剤で抑制されることも認めており、今後の研究進展が期待される。

BH-4(panic mouse)

	Cerebrum	Cerebellum	Liver
Decrease	77	6	10
Increase	7	11	19

BH-8(control mouse)

	Cerebrum	Cerebellum	Liver
Decrease	16	>300	14
Increase	2	15	13

Table 3. Numbers of genes showing 16-fold changes in gene expression just after μG flight.

謝辞：文科省科研費基盤研究A、宇宙フォーラム、厚労省科研費、武田科学振興財団助成金、アミノアップ化学助成金、住友財団環境科学助成金および医薬基盤研究所創薬等モデル動物研究プロジェクト（野村プロジェクト）の支援を受けた。

参考文献

1. Shigeki Adachi, Haruko Ryo, Tadashi Hongyo, Hiroo Nakajima, Rie Tsuboi-Kikuya, Yoriko Tokita, Fumio Matsuzuka, Keizo Hiramatsu, Kazuo Fujikawa, Tetsuo Itoh, Taisei Nomura Effects of Fission Neutrons on Human Thyroid Tissues Maintained in SCID Mice. Mutat. Res., 696,107-113 2010

2. M. Kodaira, H. Ryo, N. Kamada, K. Furukawa, N. Takahashi, H. Nakajima, T. Nomura and N. Nakamura No evidence of increased mutation rates at microsatellite loci in offspring of A-bomb survivors. Radiat. Res. 173, 205–213, 2010.

3. Taisei Nomura. Biological Consequence and Health Concern from Low Dose and Low Dose Rate Radiations in Mice and Humans. Health Physics., 2011 (in press)

4. Nomura, T., Hata, S., and Kusafuka, T. Suppression of developmental anomalies by maternal macrophages in mice. J. Exp. Med., 172: 1325-1330,1990.

5. 野村大成、梁治子、足立成基、時田偉子，堀家な緒、中島裕夫、本行忠志、藤川和男、伊藤哲夫、落合俊昌，行徳淳一郎，桂洋介。宇宙環境の人体影響評価（2009年度ワーキンググループ活動報告）。Space Utiliz Res, 26: 249-251, 2010.

Laser-driven quasi-monoenergetic proton irradiation system applied to the measurement of RBE for inactivation of human cancer cells

A. Yogo[1],* T. Maeda[1,2], T. Hori[1], H. Sakaki[1], K. Ogura[1], M. Nishiuchi[1], A. Sagisaka[1], H. Kiriyama[1], H. Okada[1], S. Kanazawa[1], T. Shimomura[1], Y. Nakai[1], M. Tanoue[1], F. Sasao[1], P. R. Bolton[1], M. Murakami[2], T. Nomura[3], S. Kawanishi[1], and K. Kondo[1]
[1]*Photo-Medical Research Center and Advanced Photon Research Center, JAEA, Kyoto 619-0215, Japan*
[2]*Hyogo Ion Beam Medical Center (HIBMC), Hyogo 679-5165, Japan and*
[3]*National Institute of Biomedical Innovation, Osaka 567-0085, Japan*

We report on the development of quasi-monoenergetic proton irradiation system driven by laser and its application to radiobiological studies. Protons accelerated by 5×10^{19}-W/cm^2 laser pulses are energy-selected by quadruple-dipole magnets (QDM) and delivered with an energy peak at 2.25 MeV and energy spread of 0.66 MeV on the full width at half maximum (FWHM). Cell survival ratio is measured with a colony formation assay for *in-vitro* cell samples from human salivary grand tumor (HSG cells) after the proton irradiation up to 8 Gy with successive bunches having a dose rate of 10^7 Gy/s. Relative biological effectiveness (RBE) for 10% survival is determined to be 1.20 ± 0.11 for 17.1 keV/μm protons, which is the first estimation for laser-accelerated ions.

Recently, interest on the application of laser-driven ion acceleration [1] to ion beam cancer therapy (IBCT) [2] has been growing rapidly because of the possibility of downsizing [3] conventional accelerators for IBCT. Including the first demonstration [4] of DNA double-strand breaking of human cancer cells by laser-driven proton beams, several experiments [5–7] have been performed from the viewpoint of investigating biological effects of short-duration and high-current beams generated with lasers. However, in the previous works [4–6] were used proton beams having wide energy spread, which is characteristics of laser-accelerated ions. Several groups successfully obtained quasi-monoenergetic ion beams using additional devices [8, 9] located downstream of their laser-driven ion sources. However, these methods have not been applied to biological studies. For quantitative estimation of biological effects, it is of crucial importance to develop a quasi-monoenergetic beam irradiation system optimally and originally designed for radiobiological investigations.

In this Letter, we report the development of laser-driven quasi-monoenergetic proton beam irradiation system using sets of miniature permanent magnets to select the beam energy. We show the first result of RBE (relative biological effectiveness) measured for inactivation of human cancer cells, which is one of the most important parameters in radiobiological studies.

The experiment was performed using the J-KAREN Ti:sapphire laser system [10] at JAEA. Figure 1 shows the setup of the ptoron beam irradiation system. The laser pulses of 1 J energy and 45 fs duration are focused to an intensity of $\sim 5 \times 10^{19}$ W/cm^2 onto a target foil of 7.5-μm-thick polyimide, which is continuously fed by a servomotor, providing a "fresh" target surface for each laser shot. The laser pulses are delivered at a repetition rate of 1 Hz. High-energy protons are accelerated from the rear surface of the target, having a continuous

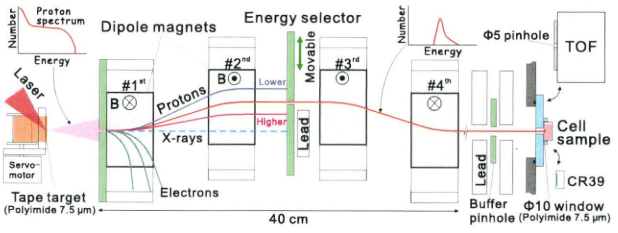

FIG. 1: Experimental setup of the laser-driven *quasi-monoenergetic* proton irradiation system.

distribution of kinetic energies up to 4 MeV.

In order to select the energy of proton beam, we have newly developed an energy-selection system using quadruple-dipole magnets (QDM), which was once simulated by Luo *et al.* [11] in their design of therapy machine assuming the use of super-conductive magnets. In the present work, each dipole magnet consists of a pair of rectangular permanent magnets, generating a central magnetic field of 0.78 T.The second and third magnetic fields are oriented antiparallel to the first and fourth ones. Protons generated from the target are collimated by the entrance pinhole and steered slightly by the first magnetic field, and again by the second one, such that transmitted proton trajectories are laterally displaced from the target normal axis by an energy-dependent distance. Then, protons having an arbitral energy is selected by a pin hole of 5 mm in diameter, the lateral position of which is moved by an electric actuator in vacuum. The energy-selected beam is again steered by the other two dipole magnets and returns onto the target normal axis. The beam shape is adjusted by a buffer pinhole and the protons are extracted from vacuum into air through a thin-foil window (10 mm in diameter) made of 7.5-μm-thick polyimide.

As depicted in Fig. 1, a capsule of cell samples is

located close to the vacuum window. The capsule has a 7.5-μm-thick cell dish made of a polyimide foil on its bottom, where cell samples originating from human salivary grand tumor (HSG cells) are cultured. Consequently protons irradiate the cells after passing through the first 7.5-μm-thick polyimide vacuum window, 3-mm of laboratory air plus the 7.5-μm-thick cell dish, keeping their kinetic energy to be high enough to penetrate the cell monolayer. For details on capsule structure and cell culture, see supplemental materials [10].

The energy of proton beams delivered from the QDM system is observed with Time-of-Flight spectrometer (TOF) [12], which enables online measurements of protons generated with a single laser shot. The TOF has a plastic scintillator (42 mm in diameter) as a detection medium, which was covered with a 5-mm-wide collimator on the detection surface during the present measurements in order to observe the proton-energy distributions exactly on the cell-sample area. Figure 2(a) shows the evidence of quasi-monoenergetic protons generated by QDM system, where the energy peak is changed from 1.5 to 3 MeV by moving the pinhole position of the energy selector laterally between 22 and 10 mm from the target normal axis.

The cell irradiation was performed with protons having energy peak of 2.25 MeV. In order to observe the shot-to-shot fluctuation of the beam current, we have measured TOF spectra for 20 successive laser shots at the beginning and the end of cell irradiation time (1-2 h). The results obtained in one experimental day are shown in Fig. 2 (b,c), where the single-shot spectra are individually shown as gray lines and their averaged spectrum is displayed as a black line. One can see that quasi-monoenergetic beam is stably generated with the 1-Hz laser operation. It should be emphasized that the energy spread of the averaged spectrum is observed to be 0.66 MeV with the full width at half maximum (FWHM). The fluctuation of proton number over the 20 shots is estimated to be $\sigma_{fluc} = 12.9\%$ and 12.3 % in standard deviation in the frame (b) and (c), respectively. This fluctuation is attributed to the stability of laser-irradiation condition that happens in a short time scale (20 s). On the other hand, the two averaged spectra show the difference of $\delta = 10.5\%$, which is coming from the fluctuation that happens in a longer time scale, *i.e.*, the time of performing one series of irradiation (1-2 h).

The areal distributions of proton number were observed before and after the cell irradiation by using track detector plates (CR-39), which were alternatively mounted on the position of cell samples. Figure 2(d) displays a scanning result of the CR-39 treated with KOH chemical etching after the proton irradiation. One can see a white spot that was induced by the bombardments of protons, the size of which corresponds to the aperture diameter (7 mm) of cell capsule. Cancer cells were located on the center of the irradiation field, which is shown with a red circle (5 mm in diameter) on the figure. The areal profile is analyzed by counting the number of proton etch-pits with a microscope along the horizontal (A-B) and vertical (C-D) lines depicted in Fig. 2(d). In Fig. 3(e) and (f), closed symbols represent the analyzed results of proton density in unit of $10^5/mm^2$, showing that the proton density is inclined. Note this profile was obtained by moving the direction of target foils slightly from the original normal axis. (All of the TOF data were obtained with this condition.) In the cell irradiation, when several shots were integrated for each sample, we rotate the capsule by 180° at the point that the half number of shot integration is finished. Thereby, we can realize homogeneous distributions of areal density as shown by solid lines in Fig. 3(e,f). As a result, the areal inhomogeneity is suppressed within $\sigma_{area} = 8.0\%$.

The absorbed dose D given by n-bunches integration is determined by the following equation:

$$D[\mathrm{Gy}] = n \int_{\mathcal{E}_0} d\mathcal{E}_0 \cdot \frac{C \cdot N(\mathcal{E}_0) \cdot E_\mathrm{d}(\mathcal{E}_0)}{Q \Delta x} \cdot 1.602 \times 10^{-7}. \quad (1)$$

Here, $C = 7.20 \times 10^4$ mm^{-2}: the areal-averaged density of proton number cross-checked by TOF and CR-39 detectors, $Q = 1$ g/cm^3: the mass density of liquid water and $\Delta x = 5$ μm: the thickness of the cell monolayer. $\mathcal{E}_0$ is the proton energy in vacuum (*i.e.* before entering the thin-foil window) and $N(\mathcal{E}_0)$ is the normalized energy distribution of protons satisfying $\int N(\mathcal{E}_0) d\mathcal{E}_0 = 1$. We determine $N(\mathcal{E}_0)$ from the averaged TOF spectrum seen in Fig. 2(b,c). $E_\mathrm{d}(\mathcal{E}_0)$ is the value of energy deposition on the cell layer in units of keV by protons having the energy $\mathcal{E}_0$. The dynamics of proton collisions are simulated with the 3-dimensional (3D) Monte-Carlo TRIM code [13]. We calculate the energy loss of protons in a multi-layer target consisting of a 7.5-μm-thick polyimide, 3-mm of air, 7.5-μm-thick polyimide as a cell dish and 5-μm of liquid water, which is assumed to be equivalent to the cell monolayer. The statistical error of proton dose is expressed by

$$\Delta D = D \sqrt{(\sigma_{fluc}^2 + \delta^2)/n + \sigma_{area}^2}, \quad (2)$$

where the first section originates from shot-to-shot fluctuation of proton number and the second one comes from the areal proton distribution. Recall $\sigma_{fluc} = 12.9\%$, $\delta = 10.5\%$ and $\sigma_{area} = 8.0\%$. Consequently, the proton dose is determined to be $D \pm \Delta D = 1.96 \pm 0.19$ for $n = 10$, for instance.

The LET (linear energy transfer) of protons are also evaluated with 3D TRIM code by calculating the energy deposition over the cell monolayer. Hence, we can obtain a volume-averaged LET accdoding to

$$LET = \int_{\mathcal{E}_0} d\mathcal{E}_0 N(\mathcal{E}_0)/\Delta x. \quad (3)$$

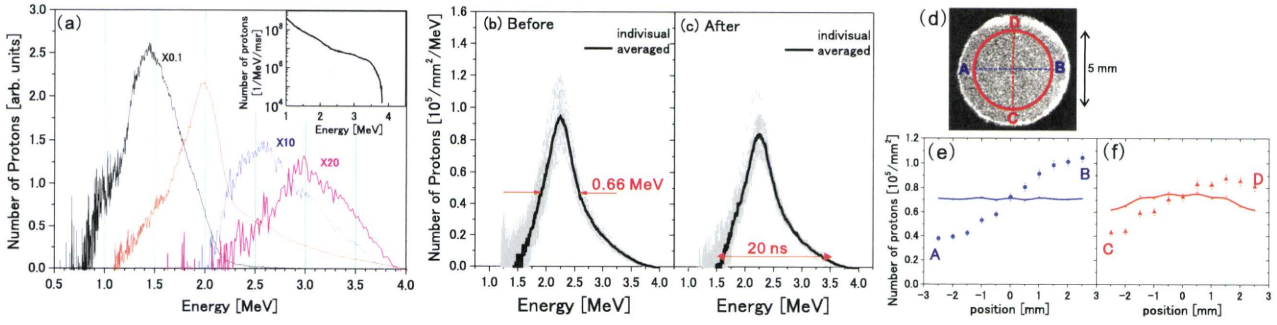

FIG. 2: (a) Results of beam-energy selection by QDM system observed with TOF spectrometer for different positions of energy-selection pinhole. The inset shows the proton-energy spectrum obtained without QDM. (b,c) Energy spectra of protons monitored at the beginning and the end of cell irradiation. (d) A beam-spot image around the cell sample position (red ciecle) measured with CR-39. (e,f) Areal densities of proton number along the axis A-B and C-D in the frame (d). The proton distributions used for the cell irradiation are shown with solid lines (see text).

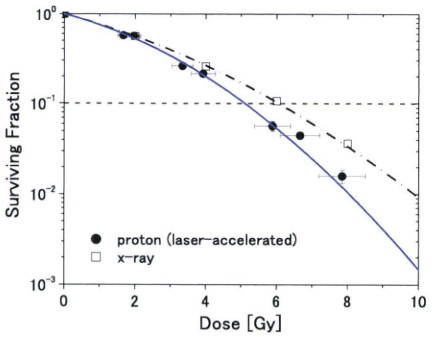

FIG. 3: The fraction of surviving cells after the irradiation with the laser-accelerated protons (closed) and a reference x-ray (open) as a function of dose. For the proton data, the statistical error ΔD is shown by horizontal bars.

Taking into account the energy spread of proton spectrum 0.66 MeV (FWHM), we determine the LET to be 17.1 ± 2.8 keV/μm.

Using a colony formation assay, we determine for the first time the value of RBE for cell inactivation by laser-accelerated ions. Figure 3 shows the fraction of surviving cells after the irradiation with the laser-accelerated protons (closed) and a reference x-ray (open) as a function of dose D up to 8 Gy. Note the x-ray was delivered from a 4-MV clinical linac at HIBMC [14]. For details, see supplemental materials [10]. The data obtained are fitted using a linear-quadratic model such that the surviving fraction (SF) is described by the equation,

$$SF = \exp\left(-\alpha D - \beta D^2\right). \tag{4}$$

By the curve fits with least-squares method, we determine the parameter values of $\alpha = 0.243 \pm 0.027$ and $\beta = 0.0409 \pm 0.0091$ for the proton data and $\alpha = 0.244 \pm 0.006$ and $\beta = 0.0224 \pm 0.0017$ for x-ray. In Fig. 3, the fit curves are shown with solid (proton) and dotted (x-ray) lines. RBE is evaluated from the dose at the 10% surviving fraction, $D_{10}(p) = 5.06$ Gy for protons and $D_{10}(\mathrm{x}) = 6.06$ Gy for x-rays. Including errors on the proton dose, we determine the RBE value to be

$$RBE = D_{10}(\mathrm{x})/D_{10}(p) = 1.20 \pm 0.11 \tag{5}$$

for the laser-accelerated protons having the volume-averaged LET of 17.1 ± 2.8 keV/μm, mentioned above.

The present RBE value is larger than those obtained with HSG cells for clinical proton beams, 1.01-1.05 [14]. This can be attributed to the fact that LET used in our condition is larger than those in the clinical Bragg-peak conditions. Further RBE measurements are necessary to discuss the effects of high dose-rate irradiation with laser-driven ions.

This work is supported by Special Coordination Funds for Promoting Science (SCF) commissioned by the Ministry of Education, Culture, Sports, Science and Technology (MEXT) of Japan.

* Electronic address: yogo.akifumi@jaea.go.jp

[1] K. W. D. Ledingham and W. Galster, New J. Phys. **12**, 045005 (2010).
[2] R. R. Wilson, Radiol. **47**, 487-491 (1946).
[3] S. V. Bulanov, T. Zh. Esirkepov, V. S. Khoroshkov, A. V. Kuznetsov, and F. Pegoraro, Phys. Lett. A **299**, 240 (2002).
[4] A. Yogo, K. Sato, M. Nishikino, M. Mori, T. Teshima, H. Numasaki, M. Murakami, Y. Demizu, S. Akagi, S. Nagayama, K. Ogura, A. Sagisaka, S. Orimo, M. Nishiuchi, A. S. Pirozhkov, M. Ikegami, M. Tampo, H. Sakaki, M. Suzuki, I. Daito, Y. Oishi, H. Sugiyama, H. Kiriyama, H. Okada, S. Kanazawa, S. Kondo, T. Shimomura, Y. Nakai, M. Tanoue, H. Sasao, D. Wakai, P. R. Bolton, and H. Daido, Appl. Phys. Lett. **94**, 181502 (2009).

[5] A. Yogo, Proceedings of IPAC ' 10, Kyoto, Japan, 91 (2010); A. Yogo *et al.*, *submitted to* Medical Physics.
[6] S. D. Kraft, C. Richter, K. Zeil, M. Baumann, E. Beyreuther, S. Bock, M. Bussmann, T. E. Cowan, Y. Dammene, W. Enghardt, U. Helbig, L. Karsch, T. Kluge, L. Laschinsky, E. Lessmann, J. Metzkes, D. Naumburger, R. Sauerbrey, M. Schurer, M. Sobiella, J. Woithe, U. Schramm and J. Pawelke, New J. Phys. **12**, 085003 (2010).
[7] T. E. Schmid, G. Dolliger, A. Hauptner, V. Hable, C. Greubel, A. Auer, A. A. Friedl, M. Molls, and B. Röper, Radiat. Res. **172**, 567 (2009).
[8] M. Nishiuchi, H. Sakaki, T. Hori, P. R. Bolton, K. Ogura, A. Sagisaka, A. Yogo, M. Mori, S. Orimo, A. S. Pirozhkov, I. Daito, H. Kiriyama, H. Okada, S. Kanazawa, S. Kondo, T. Shimomura, M. Tanoue, Y. Nakai, H. Sasao, D. Wakai, H. Daido, K. Kondo, H. Souda, H. Tongu, A. Noda, Y. Iseki, T. Nagafuchi, K. Maeda, K. Hanawa, T. Yoshiyuki, and T. Shirai, Phys, Rev. ST Accel. Beams **13**, 071304 (2010).
[9] T. Toncian, M. Borghesi, J. Fuchs, E. d'Humières, P. Antici, P. Audebert, E. Brambrink, C. A. Cecchetti, A. Pipahl, L. Romagnani, O. Willi, Science **312**, 410 (2006).
[10] *http//:.....*
[11] W. Luo, E. Fourkal, J. Li, and C.-M. Ma, Med. Phys. **32**, 794 (2005).
[12] S. Nakamura, Y. Iwashita, A. Noda, T. Shirai, H. Tongu, A. Fukumi, M. Kado, A. Yogo, M. Mori, S. Orimo, K. Ogura, A. Sagisaka, M. Nishiuchi, Y. Hayashi, Z. Li, H. Dadio, and Y. Wada, Jpn. J. Appl. Phys. Part 2 **45**, L913 (2006).
[13] J.F. Ziegler, J.P. Biersack, and M.D. Ziegler, SRIM - The stopping and Range of Ions in Matter. *SRIM Co.* (2008).
[14] K. Kagawa, M. Murakami, Y. Hishikawa, M. Abe, T. Akagi, T. Yanou, G. Kagiya, Y. Furusawa, K. Ando, K. Nojima, M. Aoki, and T. Kanai, Int. J. Radiat. Oncol. Biol. Phys. **54**, 928 (2002).